# Dimethylcuprate–Catalyzed Decarboxylative Coupling of Allyl Acetate

**ARTICLE** *in* ORGANOMETALLICS · SEPTEMBER 2012

Impact Factor: 4.13 · DOI: 10.1021/om300717g



**2 AUTHORS**, INCLUDING:

Nicole J. Rijs
Karlsruhe Institute of Technology
**16** PUBLICATIONS **298** CITATIONS

SEE PROFILE

ORGANOMETALLICS

Article

pubs.acs.org/Organometallics

# Dimethylcuprate-Catalyzed Decarboxylative Coupling of Allyl Acetate

Nicole J. Rijs and Richard A. J. O'Hair*

School of Chemistry, Bio21 Institute of Molecular Science and Biotechnology, and ARC Centre of Excellence for Free Radical Chemistry and Biotechnology, The University of Melbourne, Victoria 3010, Australia

Supporting Information

**ABSTRACT:** Allylic alkylation of organocuprates represents an important class of C−C bond forming reactions. A drawback of these reactions is their stoichiometric nature. Although metal-catalyzed decarboxylative coupling reactions offer new opportunities for formation of C−C bonds, catalytic allylic alkylation reactions of organocuprates have not been previously reported. Here, multistage mass spectrometry experiments performed on ion trap mass spectrometers in conjunction with electronic structure calculations are used to demonstrate that the dimethylcuprate anion, $[CH_3CuCH_3]^-$, can catalyze decarboxylative coupling of allyl acetate in the gas phase via a simple two-step catalytic cycle. In step 1, $[CH_3CuCH_3]^-$ undergoes a cross-coupling reaction with allyl acetate to yield $[CH_3CuO_2CCH_3]^-$ as the major product ion. Step 2 involves subjecting the product ion to collision-induced decarboxylation to re-form $[CH_3CuCH_3]^-$, thereby closing the catalytic cycle. Since the details of step 2 have been previously described (Rijs, N.; Khairallah, G. N.; Waters, T.; O'Hair, R. A. J. *J. Am. Chem. Soc.* **2008**, *130*, 1069−1079), here the focus is on step 1. Comparison of the reactivity of dimethylcuprate toward allylic susbtrates reveals that while allyl acetate reacts around 70 times more slowly than allyl iodide, it is more selective for cross-coupling. This is rationalized by DFT calculations, which reveal that an increase in kinetic barrier is responsible for both reactivity trends. The lowest energy path was found to involve a stepwise $\pi$-oxidative addition proceeding via an $\eta^2$-$C_3H_5O_2CCH_3$ intermediate and extrusion of a leaving group (LG) anion, followed by a reductive elimination where this LG is recomplexed to the copper center. Finally, DFT calculations were used to shed light on the role of leaving groups LG = $CH_3CO_2^-$, $I^-$, $Br^-$, $Cl^-$ in the allylic alkylation. While selectivity is indeed achieved at the cost of reactivity, the LG effects were more complex than can be accounted for by a simple consideration of the anion proton affinity (APA) of the LG.

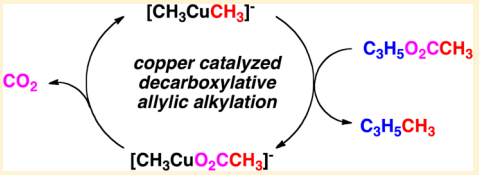


## INTRODUCTION

From a green chemistry perspective, decarboxylative coupling is a highly desirable process in terms of atom economy, since neutral extrusion of carbon dioxide from an ester enables C−C bond formation (eq 1).[1] Unfortunately, direct thermolysis of

$$RCO_2R' \rightarrow R{-}R' + CO_2 \quad (1)$$

esters typically yields a mixture of products.[2] Decarboxylative cross-coupling is the process of neutral extrusion of carbon dioxide from a carboxylate feedstock (for example, a carboxylic acid or salt) to form an active organometallic species which can participate in cross-coupling (eq 2).[3] Metals used to catalyze

$$RCO_2H + R'X \xrightarrow{\text{cat.}} R{-}R' + CO_2 + HX \quad (2)$$

decarboxylative cross-coupling reactions commonly include the group 11 metals, palladium and rhodium.[3b] A wide range of functionality on the carboxylate (R) is tolerated, making this a versatile method for C−C coupling. Allylic and benzylic esters are readily employed as substrates in such catalytic decarboxylative reactions (eq 2, R′ = allyl, benzyl; X = carboxylate group).[4] In one of the earliest examples of such a reaction, Steglich and co-workers used intramolecular decarboxylative cross-coupling catalyzed by palladium(II) acetate in the final step of the biomimetic synthesis of the marine alkoloid lamellarin G trimethyl ether.[5a] More recently, decarboxylative coupling of biaryls has led to an array of biologically active compounds.[5b]

As highlighted previously,[6] allylic alkylations are an important class of copper-mediated reaction, useful in constructing many commercially and biologically important molecules.[7] We recently examined the gas-phase reactions of group 11 dimethylmetalates with allyl iodide and found that dimethylcuprate promoted a cross-coupling reaction, with concurrent formation of a methylcopper iodide anion by-product, $[CH_3CuI]^-$ (eq 3, LG = $I^-$). These reactions were

$$[CH_3CuCH_3]^- + C_3H_5LG \rightarrow [CH_3CuLG]^- + CH_3C_3H_5 \quad (3)$$

carried out in an ion trap mass spectrometer, where $[CH_3CuCH_3]^-$ was formed via double decarboxylation of $[CH_3CO_2CuO_2CCH_3]^-$ using collision-induced dissociation (CID).[8]

**Special Issue:** Copper Organometallic Chemistry

**Received:** July 27, 2012

   dx.doi.org/10.1021/om300717g | *Organometallics* XXXX, XXX, XXX−XXX

It occurred to us that the allylic alkylation process could be made catalytic by changing the leaving group (LG) from iodide to acetate, thereby closing the catalytic cycle by re-forming the active species **1** (Scheme 1.).

**Scheme 1. Proposed Two-Step Catalytic Cycle for the Dimethylcuprate Catalyzed Decarboxylative Coupling of Allyl Acetate**

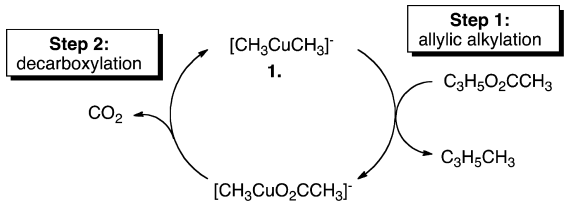


Thus, an extension to organocuprate-catalyzed decarboxylative allylic alkylations would combine the power of copper in (i) mediating nucleophilic substitution reactions with convenient substrates bearing carboxylate leaving groups and (ii) catalyzing decarboxylation reactions to form organocopper complexes.[3,5b] With regard to the first point, reactions between allylic esters and cuprates have been known for more than 40 years.[9] The stereoselectivity of these reactions was noted early on,[10] along with the potential intermediacy of $\pi$-allyl intermediates.[11] The mechanism of reaction between allyl acetate and dimethylcuprate has been examined computationally by Nakamura and co-workers.[12] While a detailed analysis of the bimetallic cuprate/lithium species was undertaken, only a limited study of the intrinsic reactivity of the bare dimethylcuprate anion toward allyl acetate was considered. In this reaction, the kinetic barrier was found to be significantly above the level of the separated reactants, and thus no reaction would be expected to take place. However, the assistance or possible transfer of the carboxylate leaving group was not reported. These coupling reactions are stoichiometric, and the organocuprate-catalyzed decarboxylative coupling of allyl esters has hitherto not been reported. With regard to the second point, copper-catalyzed protodecarboxylation reactions have been extensively used in organic synthesis since they were first reported by Shepard et al. in 1930,[5c] and using a combination of mass spectrometry experiments and DFT calculations, we have examined the gas-phase decarboxylation reactions of a range of copper(I) carboxylate complexes, including the mechanism and energetics for the formation of $[CH_3CuCH_3]^-$ from $[CH_3CuO_2CCH_3]^-$ (step 2 of Scheme 1).[8]

Previous studies have highlighted that catalytic cycles can be studied in in the gas phase.[13] Using multistage mass spectrometry experiments, catalytic intermediates or byproducts may be isolated, and their unimolecular or bimolecular reactivity can be probed.[13] In conjunction with theoretical modeling this approach can illuminate the mechanisms of the various steps involved in catalysis.

Given the fact that the bare dimethylcuprate anion has been shown to react with allyl iodide (described above, eq 3) and the iodide anion has been shown to assist allylic alkylation by lowering reaction barriers,[6] the aim of the work described here is to (i) establish whether bare dimethylcuprate anion reacts with allyl acetate in an allylic alkylation reaction in the gas phase, (ii) determine whether the leaving group ($CH_3CO_2^-$) is transferred to the copper center for subsequent regeneration of the catalytically active species, (iii) use DFT calculations to predict the most likely reaction mechanism for allylic alkylation, and (iv) compare the effects of acetate versus halide leaving groups in allylic alkylation reactions.

## EXPERIMENTAL SECTION

**Reagents.** Copper(II) acetate and allyl acetate were obtained from Aldrich. Acetic acid-$d_4$ was obtained from Cambridge Isotope Laboratories. All chemicals were used without further purification.

**Mass Spectrometry.** Ion−molecule reactions (IMR) were performed on a modified Finnigan LCQ quadrupole ion trap mass spectrometer equipped with a Finnigan ESI (electrospray ionization) source, as previously described.[14] Additional IMR were performed in a Thermo Finnigan LTQ linear ion trap mass spectrometer.[15] Gronert has shown that the temperature of ions trapped in an ion trap mass spectrometer without ion activation are at near-thermal conditions (i.e., room temperature).[14c]

Accurate mass measurements were conducted using the FT-MS to establish the stoichiometry of product ions derived from the ion−molecule reactions, as previously described.[15] Methanolic solutions of copper(II) acetate with concentrations of 0.5−1.0 mM were injected into the ESI source at a flow rate of 5 $\mu$L/min. Typical electrospray source conditions involved needle potentials of 3.5−4.5 kV and a heated capillary temperature of 180 °C. Mass selection, collisional activation, and ion−molecule reactions were carried out using the "advanced scan" function of the LCQ software, which allows the Q value and the reaction time to be varied. The neutral substrate allyl acetate was introduced at various concentrations into the ion trap via the helium inlet line. Rates were measured by varying the time delay between isolation of the $[CH_3CuCH_3]^-$ reactant ion and its mass analysis ("Reaction Delay", RD). The decay of $[CH_3CuCH_3]^-$ was monitored over at least six values of RD. The intensity of the reactant ion was calculated by integration of its ion count within the mass-selected window. Pseudo-first-order rates were estimated by extrapolation of plots of $-\ln((([CH_3CuCH_3]^-$ intensity)/(total ion intensity)) vs RD. Rate constants were calculated by dividing the pseudo-first-order rate coefficient by the calculated concentration of allyl acetate in the ion trap. The rate constants and branching ratios reported are the average of at least five independent measurements conducted on at least four separate days.[16] Standard deviations in rate constants were typically around 30%. A conservative estimate of error is ±25%, but relative rates are expected to be more accurate due to cancellation of errors.

Collision rates were calculated via the average dipole orientation (ADO) theory of Su and Bowers using the COLRATE program.[17]

**Theoretical Calculations.** Theoretical calculations were carried out to provide insights into the bimolecular and catalytic reactivity of the dimethylcuprate. Gaussian 09,[18] utilizing the B3LYP hybrid functional,[19] was used for all geometry optimizations and vibrational frequency calculations. The Stuttgart Dresden (SDD) basis set and effective core potential (ECP) were used for the copper atoms, while the 6-31+G(d) all-electron basis set was used for carbon, hydrogen, and oxygen.[20] Optimized B3LYP geometries of organocuprate complexes were previously compared with those determined from X-ray crystallography.[8] There was excellent structural agreement between the calculated geometries and those determined experimentally. Thus, this combination of method and basis set was chosen, as it predicts structures well. All transition-state (TS) geometries were characterized by the presence of a single imaginary frequency, and intrinsic reaction coordinates (IRC) were examined to ensure smooth connection of reactants and products. The energetics presented were calculated with B3LYP utilizing the larger Def2-QZVP basis set (C, H, O, all electron; Cu, including ECP),[21] defined as B3LYP/Def2-QZVP//B3LYP/SDD6-31+G(d). All quoted relative energies ($E_0$) include zero point vibrational energy (unscaled) calculated at the optimization level and are not corrected for basis set superposition error.

To assess the robustness of B3LYP energetic trends, key stationary points were calculated with the M06 functional[22] and the B2PLYPD double hybrid functional[23] (Supporting Information, Table S1). For the allyl acetate system, the predicted energetic trends are entirely consistent among all three methods. Thus, as these trends were also


dx.doi.org/10.1021/om300717g | Organometallics XXXX, XXX, XXX−XXX

**Scheme 2. Generation and Potential Gas-Phase Ion−Molecule Reactions of Dimethylcuprate with Allyl Acetate**

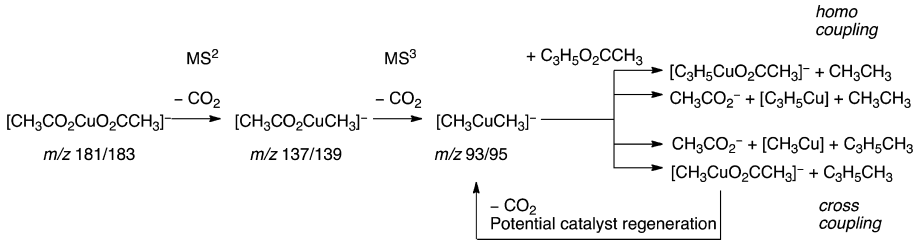


consistent between these methods for allyl iodide, the subsequent leaving group comparisons are made with B3LYP derived energies.

Visualizations of the molecules appearing in this report were created using MacMolPlt.[24]

## RESULTS AND DISCUSSION

**Experimental Results.** Dimethylcuprate precursor ions were generated via multistage mass spectrometry methods using a double-decarboxylation strategy. Decarboxylation of copper carboxylate was promoted by CID (Scheme 2). As this process has been described in detail in previous reports,[8] here the focus is on establishing how dimethylcuprate reacts with allyl acetate, and whether the catalytic cycle shown in Scheme 1 operates.

The IMR were conducted in an $MS^4$ experiment in a fashion analogous to that previously described[6] by allowing the mass-selected $^{63}Cu$ dimethylcuprate anion ($m/z$ 93) to react with allyl acetate (Scheme 2). These reactions were also undertaken with the isotopologues $d_3$-dimethylcuprate and $d_6$-dimethylcuprate ($m/z$ 96 and 99, respectively). Since the neutral products of ion−molecule reactions are not detected in our experiments, they are inferred from the detected ionic products.[6] The resultant IMR spectra are shown in Figure 1. Figure 1a reveals that a substitution reaction takes place with allyl acetate, according to eq 4, forming the product $[CH_3CuO_2CCH_3]^-$ ($m/z$ 137).

$$[CH_3CuCH_3]^- + C_3H_5O_2CCH_3 \rightarrow [CH_3CuO_2CCH_3]^- + C_3H_5CH_3 \quad (4)$$

The results of deuterium labeling experiments (Figure 1b,c) confirm the assignment that substitution involves the acetate group from the allyl acetate neutral, according to eqs 5 and 6.

$$[CD_3CuCH_3]^- + C_3H_5O_2CCH_3 \rightarrow [CH_3CuO_2CCH_3]^- + C_3H_5CD_3 \quad (5a)$$

$$\rightarrow [CD_3CuO_2CCH_3]^- + C_3H_5CH_3 \quad (5b)$$

$$[CD_3CuCD_3]^- + C_3H_5O_2CCH_3 \rightarrow [CD_3CuO_2CCH_3]^- + C_3H_5CD_3 \quad (6)$$

The results for the $^{65}Cu$ isotope (shown in the Supporting Information, Figure S1) also confirm this reactivity. Thus, $[CH_3CuO_2CCH_3]^-$ is the product ion arising from C−C bond formation via cross-coupling of a cuprate methyl group with the allylic substrate (Scheme 1). A comparison of integrated ion abundances of the product ions $[CH_3CuO_2CCH_3]^-$ ($m/z$ 137) and $[CD_3CuO_2CCH_3]^-$ ($m/z$ 140) formed in the competing cross-coupling reactions of $[CD_3CuCH_3]^-$ (eqs 5a and 5b)

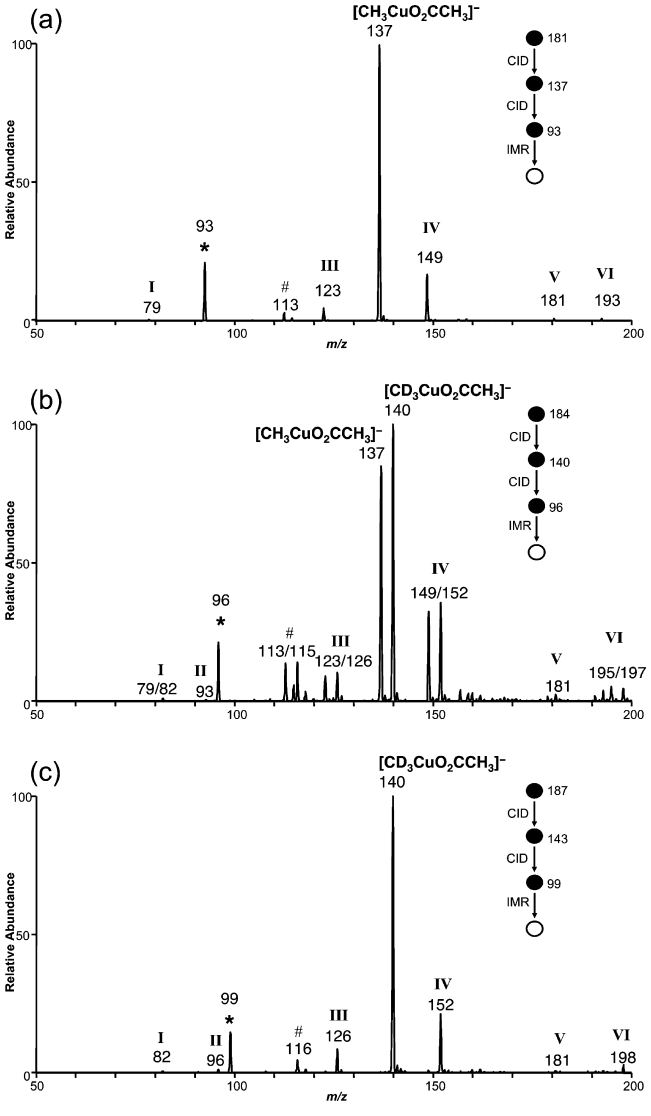


**Figure 1.** $MS^4$ mass spectra showing ion−molecule reactions among allyl acetate ($C_3H_5O_2CCH_3$) and (a) dimethylcuprate anion $[CH_3{}^{63}CuCH_3]^-$ ($m/z$ 93), (b) $d_3$-dimethylcuprate anion $[CD_3{}^{63}CuCH_3]^-$ ($m/z$ 96), and (c) $d_6$-dimethylcuprate anion $[CD_3{}^{63}CuCD_3]^-$ ($m/z$ 99). The mass-selected ion is marked with an asterisk in each spectrum. The peaks I−VI correspond to primary and secondary products, while # denotes $[CH_3{}^{63}CuCl]^-$.

allows the determination of a secondary deuterium kinetic isotope ($k_H/k_D$) effect of 1.2 ± 0.1, which is essentially identical with that determined for the allylic alkylation reaction with allyl iodide.[6,25]

The peaks denoted with roman numerals (I−VI) in Figure 1 are other primary or secondary products, and their masses were


dx.doi.org/10.1021/om300717g | Organometallics XXXX, XXX, XXX−XXX

confirmed via accurate mass FT-MS (Supporting Information, Table S2). Suggested assignments based on the isotopic masses, where X = H, D, are as follows: (I) $[CX_3CuH]^-$, (II) $[CH_3CuCX_3]^-$, (III) $[CX_3CuO_2CH]^-$, copper formate, (IV) $[CX_3Cu(C_3H_3O_2)]^-$ (where $C_3H_3O_2$ is an empirical formula), (V) $[CH_3CO_2CuO_2CCH_3]^-$, (VI) $[CX_3CuCX_2(C_3HO_4)]^-$ or $[CX_3CuCX_2(C_4H_5O_3)]^-$, where $C_3HO_4$ and $C_4H_5O_3$ are empirical formulas. Another minor peak (see Table S2), was found to be (VII) $[CH_3Cu(C_7H_{11}O_2)]^-$. The origin of # is most likely due to a minor chloride contamination in the IMR line (i.e., # = $[CX_3CuCl]^-$). Two secondary products were established as $[CH_3CO_2CuO_2CCH_3]^-$ ($m/z$ 181, V) and $[CH_3CuCX_3]^-$ (II), the former due to a second coupling reaction and the latter resulting from decarboxylation of the product ion $[CX_3CuO_2CCH_3]^-$ (X = H, D) (eq 7 and Figure 2).

$$[CX_3CuO_2CCH_3]^- \rightarrow [CX_3CuCH_3]^- + CO_2 \quad (7)$$

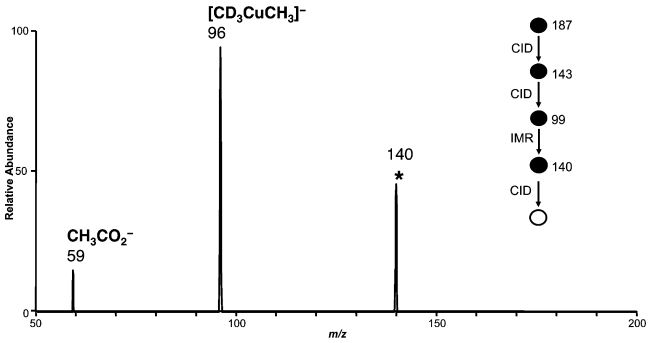


**Figure 2.** $MS^5$ spectra, IMR of $[CD_3CuCD_3]^-$ with allyl acetate (Figure 1c) resulting in $[CD_3CuO_2CCH_3]^-$ ($m/z$ 140). CID on this ion at $m/z$ 140 results in decarboxylation (the mass difference of 44 corresponds to loss of $CO_2$ (eq 7)).

A careful analysis of the temporal evolution of the product ions allowed the branching ratios of the primary product ions for the reaction of allyl acetate and dimethylcuprate ($m/z$ 93) to be established (Table 1). While the mechanistic origins of the ions $[CH_3CuO_2CH]^-$ (III) and $[CH_3Cu(C_3H_3O_2)]^-$ (IV) have unfortunately not been established, two key points are that (i) the product ion at $m/z$ 137, methylcopper acetate $[CH_3CuO_2CCH_3]^-$, is the most abundant ionic product (81%) and (ii) CID on the product ion at $m/z$ 140 formed via IMR in Figure 1c results in decarboxylation according to eq 7, where X = D (Figure 2), confirming that the reactive dimethylcuprate species $[CH_3CuCH_3]^-$ may be re-formed thermally and thus closes the catalytic cycle (Scheme 1, step 2).

**Table 1. Branching Ratios of Product Ions for the Gas-Phase Ion−Molecule Reaction of Allyl Acetate with Dimethylcuprate ($m/z$ 93)**

| assignment | mass ($m/z$) | branching ratio (%)[a] |
|---|---|---|
| $[CH_3CuO_2CH]^-$ (III) | 123 | 4 |
| $[CH_3CuO_2CCH_3]^-$ | 137 | 81 |
| $[CH_3Cu(C_3H_3O_2)]^-$ (IV) | 149 | 15 |

[a]Only the identifiable primary products were included in these branching ratio measurements.

An interesting aspect of the allyl acetate substrate reactivity with dimethylcuprate is the absence of two classes of product observed for the related allyl iodide system. While allyl iodide reacts via homocoupling to produce $[C_3H_5CuI]^-$,[6] the related homocoupling product ion, $[C_3H_5CuO_2CCH_3]^-$, is not observed at $m/z$ 163. Thus, the allyl acetate substrate appears to be selective for cross-coupling. The other conspicuously absent product ion is the leaving group anion, which would otherwise be visible at $m/z$ 59 ($CH_3CO_2^-$). The iodide anion ($m/z$ 127) is a prominent feature of the IMR spectra of dimethylcuprate reacting with allyl iodide.[6] DFT calculations suggested that $I^-$ can be formed via multiple mechanistic pathways. However, the absence of $CH_3CO_2^-$ in the spectra in Figure 1 suggests that the acetate leaving group is sequestered by the copper center in the allylic alkylation reaction. This is a promising feature, as the potential precursor to the catalytic species (Scheme 1), the acetate ligand, is not lost.

The kinetics for the IMR of $[CH_3CuCH_3]^-$ with allyl acetate were measured. The rate of reaction ($k_{measured}$) was determined to be $(11 \pm 4) \times 10^{-13}$ cm$^3$ molecule$^{-1}$ s$^{-1}$ (the error corresponds to 1 standard deviation), which translates to a modest reaction efficiency of 0.032% (the collision rate, $k_{ADO}$, is estimated to be $3.44 \times 10^{-9}$ cm$^3$ molecule$^{-1}$ s$^{-1}$). Indeed, the reaction with allyl acetate is more that 70 times slower than that for allyl iodide. Thus, changing the LG to acetate slows the allylic alkylation reaction.

These experimental results show that, while allyl acetate is significantly slower to react than allyl iodide, the reaction is more selective. Conservation of the leaving group is of prime importance for setting up the catalytic precursor, $[CH_3CuO_2CCH_3]^-$, to dimethylcuprate. Indeed, $[CH_3CuO_2CCH_3]^-$ is readily decarboxylated, as shown both by small amounts of secondary products being formed in the exothermic ion−molecule reaction (Figure 1) and by CID of the mass selected product ion (Figure 2). Thus, the gas-phase catalytic cycle for the dimethylcuprate-catalyzed decarboxylative coupling of allyl acetate has been experimentally established (Scheme 1). In the next section the most likely reaction mechanism and the effect of the leaving groups on the allylic alkylation reaction (step 1 of Scheme 1) are determined via the use of DFT calculations.

**Computational Results.** The results of the gas-phase IMR of dimethylcuprate with allyl acetate revealed the re-formation of the copper carboxylate species, suggesting that cross-coupling occurs. In addition, the reaction was more than 70 times slower for allyl acetate than for allyl iodide. Electronic structure calculations were undertaken to gain insight into the most viable reaction mechanisms and the origin of these differences in reactivity.

The pathways analyzed here were informed by our previous work on allyl iodide:[6] concerted nucleophilic substitution at the $S_N2'$ (Scheme 3, path A, $\gamma$-carbon) or $S_N2$ (Scheme 3, path B, $\alpha$-carbon) position; stepwise $\sigma$-type oxidative addition ($\alpha$-carbon) followed by reductive elimination (Scheme 3, path C) and stepwise $\pi$-type oxidative addition followed by reductive elimination (Scheme 3, path D, $\gamma$-carbon) resulting in cross-coupling. The potential for homocoupling via the M(III) intermediate formed in path D was also examined. The leaving group (LG) was found to alter the mechanism of $\pi$-type oxidative addition, and this will be discussed in more detail. A key criterion for establishing the likely mechanism(s) of the reaction is the recognition that the near-thermal conditions of ion−molecule reactions in an ion trap mass spectrometer[14c] dictates that the barrier(s) should be below the level of the energy of the separated reactants. As chemical accuracy is not expected to be met with the B3LYP computational method, the pathways which are close to or below the energy of the separated reactants will be considered viable under the experimental conditions used. As noted in the Experimental Section, additional calculations were


dx.doi.org/10.1021/om300717g | Organometallics XXXX, XXX, XXX−XXX

**Scheme 3. Potential Mechanistic Pathways A–D**[a]

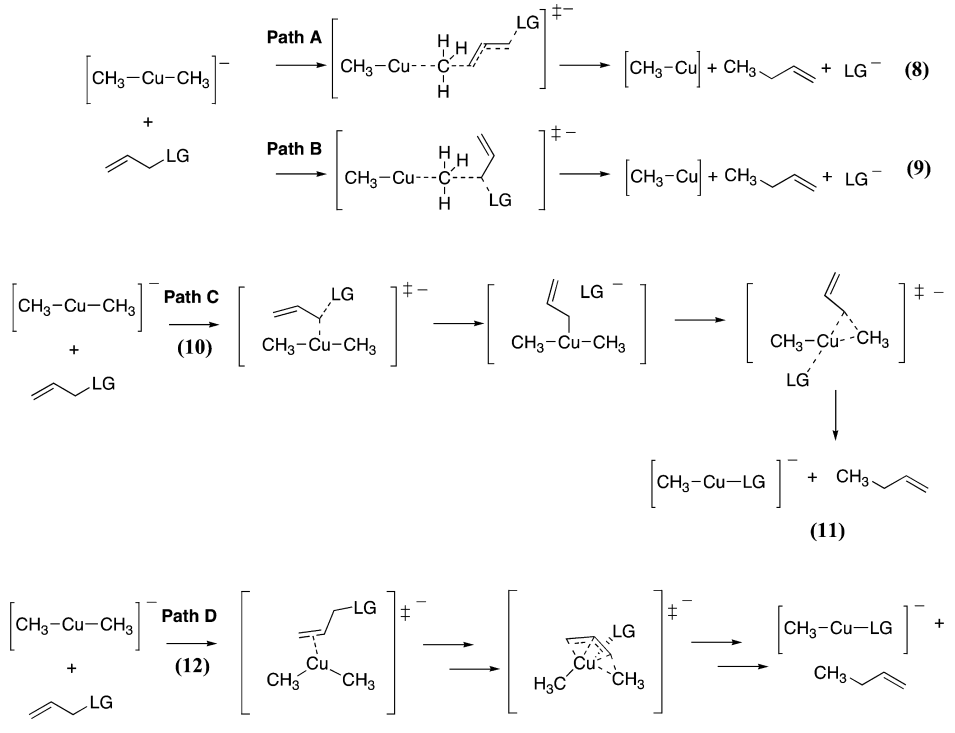


[a]LG = leaving group (acetate).

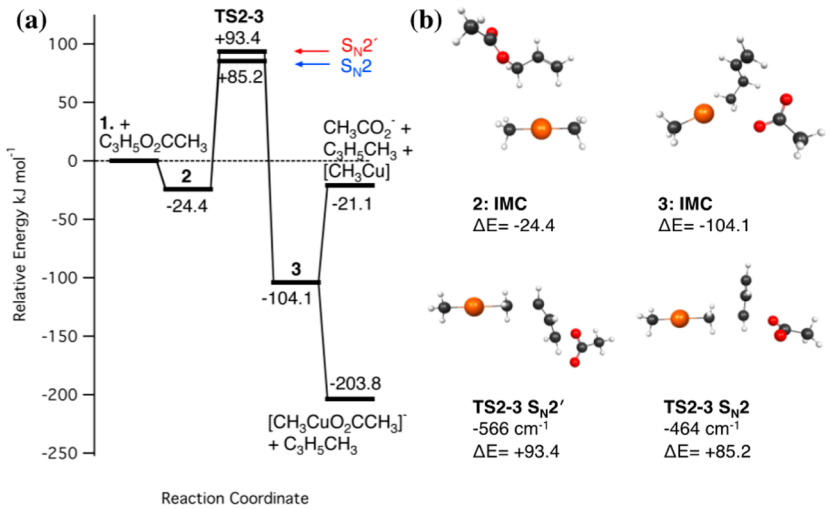


**Figure 3.** Calculated B3LYP/Def2-QZVP//B3LYP/SDD6-31+G(d): (a) relative energies (kJ $mol^{-1}$) for minima and transition states relevant to bimolecular reactions of $[CH_3CuCH_3]^-$ + $C_3H_5O_2CCH_3$ via paths A and B; (b) structures of minima and transition states relevant to the bimolecular reactions of $[CH_3CuCH_3]^-$ + $C_3H_5O_2CCH_3$ via paths A and B of Scheme 3.

carried out using other computational methods in order to evaluate the predicted trends in the relative energetics for the different mechanisms shown in Scheme 3. These show that pathway D has the lowest energy barriers for all methods used (see the Supporting Information, Table S1). In the next sections, each of the mechanistic pathways are discussed in detail.

*Paths A and B.* Both concerted nucleophilic substitution paths A and B ($S_N2'$ and $S_N2$; Scheme 3, eqs 8 and 9) have high kinetic barriers (Figure 3, 93.4 and 85.2 kJ $mol^{-1}$). Despite being exothermic overall, these reactions are not expected to occur under the experimental conditions of the ion trap.

The TS geometries for paths A and B (Figure 3, **TS2-3**) are structurally similar to those found for LG = iodide. The TS vibration shows inversion of the hydrogen atoms on the methyl group of the cuprate undergoing C–C bond formation, plus simultaneous elimination of the acetate leaving group. These TS geometries do not give a direct transfer of $LG^-$ ($CH_3CO_2^-$) to the copper center. The opportunity to form $[CH_3CuO_2CCH_3]^-$ is available via IMC **3**; however, free $LG^-$ is expected to be observed in the mass spectrum should these $S_N2$ or $S_N2'$ mechanisms be occurring. This is not the case, since $CH_3CO_2^-$ is not observed in Figure 1. Thus, the combination of experiment and


dx.doi.org/10.1021/om300717g | *Organometallics* XXXX, XXX, XXX–XXX

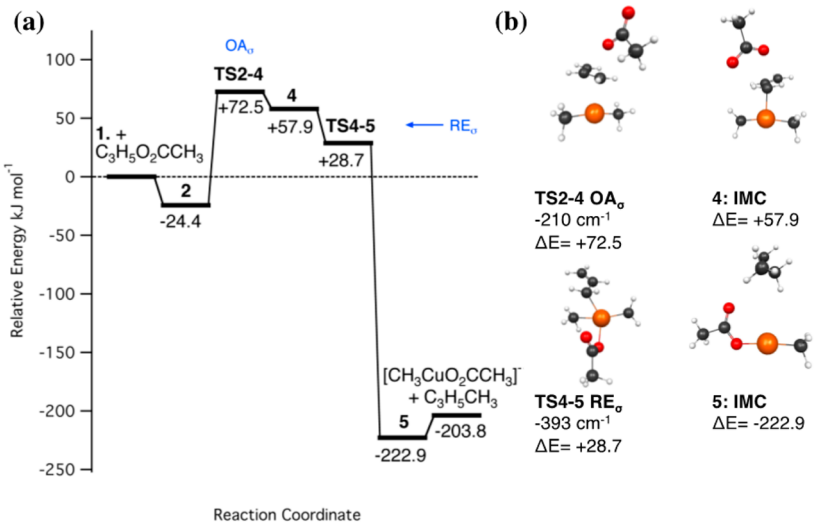


**Figure 4.** Calculated B3LYP/Def2-QZVP//B3LYP/SDD6-31+G(d): (a) relative energies (kJ mol$^{-1}$) for minima and transition states relevant to bimolecular reactions of $[CH_3CuCH_3]^-$ + $C_3H_5O_2CCH_3$ via path C ($\sigma$ oxidative addition); (b) structures of minima and transition states relevant bimolecular reactions of $[CH_3CuCH_3]^-$ + $C_3H_5O_2CCH_3$ via path C of Scheme 3.

theory suggest that paths A and B are not the preferred cross-coupling mechanisms to yield $[CH_3CuO_2CCH_3]^-$.

*Path C.* The stepwise $\sigma$-oxidative addition/reductive elimination cross-coupling pathway, path C (Scheme 3), also has a substantial kinetic barrier (**TS2-4**; Figure 4, 72.5 kJ mol$^{-1}$). Thus, oxidative addition via this pathway (Scheme 3, eq 10) is not expected to occur experimentally.

The structure of the TS of OA$_\sigma$ for LG = acetate is analogous to that of LG = iodide, involving very little bend from linearity of the cuprate and an $S_N2$-like TS vibration of the M−C bond forming groups, though the kinetic barrier is significantly higher in energy than that of the latter (−37.5 versus 72.5 kJ mol$^{-1}$, respectively). The TS for RE$_\sigma$ follows a similar trend, where the geometries are similar to those previously analyzed (the typical RE geometry found for methyl iodide[26] and RE$_\sigma$ allyl iodide).[6] However, the energy is increased for the acetate leaving group (compare $C_3H_5$LG TS RE$_\sigma$, LG = I$^-$, −37.5 kJ mol$^{-1}$ to LG = $CH_3CO_2^-$, 28.7 kJ mol$^{-1}$).

The cross-coupling reaction via path C is dependent on (1) the LG anion being an effective leaving group (i.e., the stability of the anion) and (2) the Lewis basicity of the anion being appropriate for assisting the RE$_\sigma$ process. The gas-phase anion proton affinity (APA, eq 13) of $CH_3CO_2^-$ is 1456 versus 1315.24 kJ mol$^{-1}$ for I$^-$,[27] indicating the latter is a weaker base and a better leaving group. This appears to correlate with the energetic trend to OA$_\sigma$. In terms of (2), I$^-$ is a soft base and $CH_3CO_2^-$ is a hard base.[28] It is less clear what role this plays in assisting or stabilizing the RE TS at the copper center. A combination of anion size (and hence bond length), basicity, and polarization effects are likely to play a role. It is observed that iodide is superior in reactivity to acetate via this cross-coupling mechanism, due to possessing lower kinetic barriers; however, acetate is more likely to be transferred to the copper center as a ligand.

$$LG^- + H^+ \rightarrow H{-}LG \quad \Delta H_{rxn} = APA \tag{13}$$

*Path D.* The lowest energy pathway for a cross-coupling reaction between allyl acetate and dimethylcuprate is path D (Scheme 3). An examination of path D reveals three potential

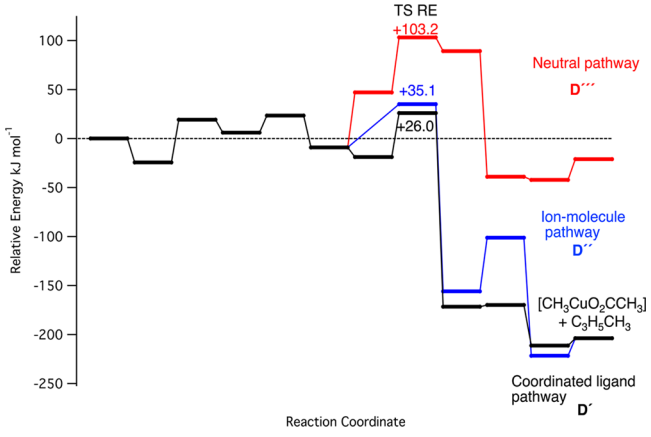


**Figure 5.** Comparison of cross-coupling pathways via $\pi$-oxidative addition and reductive elimination. Energies of limiting kinetic barrier (TS RE$_\pi$) are annotated, while others are omitted for simplicity.

mechanisms to cross-coupling (Scheme 4), dependent on the role of the LG.

A $\pi$-oxidative addition (**TS2-6**) results in an $\eta^2$-($C_3H_5O_2CCH_3$) intermediate, **6**. Subsequently, there is a LG elimination (**TS6-7**); thus, the $\eta^3$-($C_3H_5$) intermediate is formed in a stepwise manner. This is unlike $\pi$-oxidative addition with LG = iodide, where the $\eta^3$-($C_3H_5$) intermediate is formed in a process that is concerted with respect to the loss of the LG (Figure 6a in ref 6). Thus, the Cu(III) IMC **7** is formed in a stepwise OA$_\pi$ fashion.

Three alternatives to cross-coupling are then possible via **7** (Scheme 4): path D′, where the LG interacts with metal leading to RE, path D″, where the LG forms an ion−molecule complex resulting in RE and the same products as for D′, and path D‴, where LG dissociates and neutral product completes RE without. The latter neutral pathways have been previously explored[12] and, since they are energetically demanding, are unlikely to occur.

This is clearly shown in Figure 5, where TS RE from a neutral pathway has a kinetic barrier of 103.2 kJ mol$^{-1}$ and is the kinetically least favorable of all the cross-coupling paths examined thus far. The other two RE$_\pi$ options are lower in energy and are thus more viable. The ion−molecule pathway, TS RE$_\pi$ D″, has a kinetic barrier of 35.1 kJ mol$^{-1}$ and also has


dx.doi.org/10.1021/om300717g | *Organometallics* XXXX, XXX, XXX−XXX

**Scheme 4. Mechanistic Pathways to Cross-Coupling via $\pi$-Oxidative Addition and Reductive Elimination (Path D)**

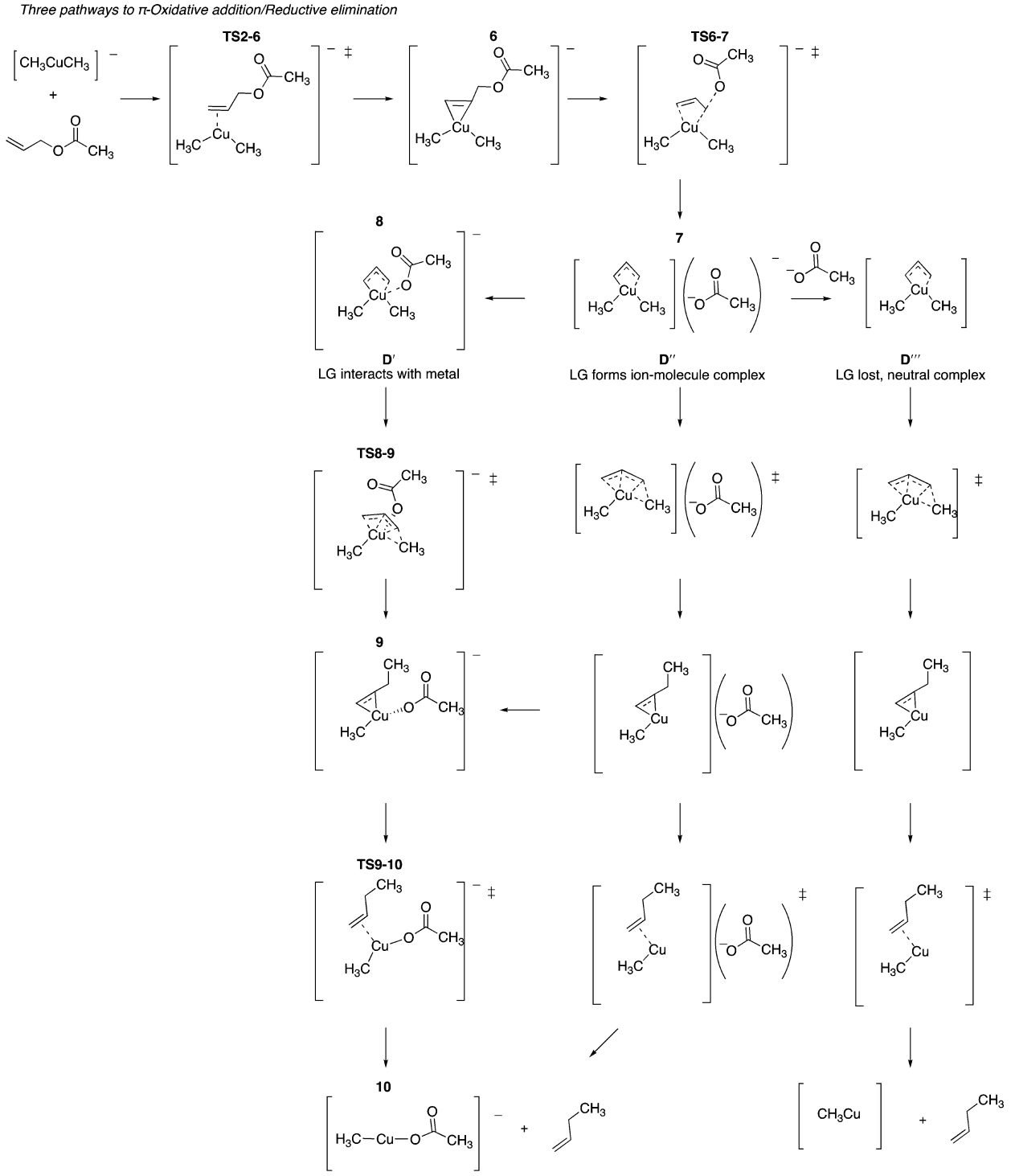


the opportunity to form a coordinating LG ligand. The ligand-coordinated mechanism, D′, has the lowest energy with a barrier of 26.0 kJ mol$^{-1}$ and will be discussed in more detail.

Figure 6 shows the energy of all the consecutive steps involved in $\pi$-OA/RE via path D, along with the reaction structures. The TS barriers to $OA_\pi$, LG dissociation, and $RE_\pi$ are 19.2, 23.4, and 26.0 kJ mol$^{-1}$, respectively, followed by a low-lying TS for olefin elimination (−169.8 kJ mol$^{-1}$). These are far lower barriers (by 50−70 kJ mol$^{-1}$) than for any of the other cross-coupling paths A−C (Scheme 3) and thus represent the most likely reaction mechanism for allylic substitution involving allyl acetate. The TS geometries for $RE_\pi$ are similar to those examined for LG = iodide; however, the acetate group is interacting with the copper center to a greater extent than the iodide (compare ref 6 **TS9-10**, Figure 4, with this work, **TS8-9**, Figure 6). This is very clearly shown by the Cu−LG distances in the TS $RE_\pi$ (Cu−I = 5.25 Å versus Cu−O = 2.26 Å).

Thus, the LG is stabilizing the RE TS in the two viable pathways of Scheme 4 and is transferred to the copper center. There is no opportunity for LG loss, which is consistent with


dx.doi.org/10.1021/om300717g | *Organometallics* XXXX, XXX, XXX−XXX

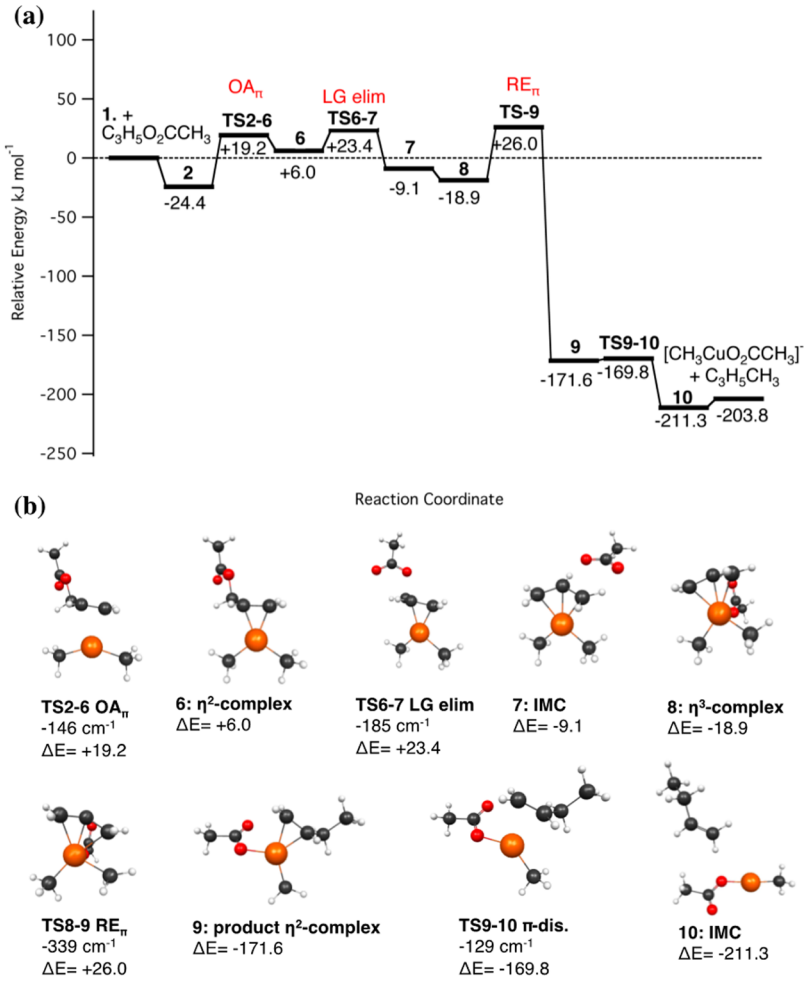


**Figure 6.** Calculated B3LYP/Def2-QZVP//B3LYP/SDD6-31+G(d): (a) relative energies (kJ mol$^{-1}$) for minima and transition states relevant to bimolecular reactions of $[CH_3CuCH_3]^-$ + $C_3H_5O_2CCH_3$ via path D ($\pi$-addition) of Scheme 3; (b) structures of minima and transition states relevant to bimolecular reactions of $[CH_3CuCH_3]^-$ + $C_3H_5O_2CCH_3$ via path D ($\pi$-addition) of Scheme 3.

the absence of $CH_3CO_2^-$ in the IMR spectra (Figure 1). Though the carboxylate anion assists in stabilizing the TS RE, it does not lower the reaction barrier by the same magnitude as a participating iodide anion does (26.0 versus −45.4 kJ mol$^{-1}$, respectively). Though this pathway is the lowest energy and thus the most viable pathway for cross-coupling, it resides above the energy of the separated reactants. However, the DFT method used is not expected to attain absolute chemical accuracy when considering TS barriers. Indeed, the barriers drop on moving to the M06 and B2PLYPD methods, with the latter below the energy of the separated reactants (see the Supporting Information Table S1). Thus, in the absence of lower energy pathways, path D is the most likely mechanism for the cross-coupling reaction inferred from the experiments.

*Homocoupling via Path D.* In the IMR experiments with allyl acetate, the ionic product, $[C_3H_5CuO_2CCH_3]^-$, from the homocoupling pathway was not observed (Figure 1). Given that the homocoupling product was observed during IMR between dimethylcuprate and allyl iodide,[6] calculations were carried out to find the origin of this difference in reactivity. Figure 7 reveals that the kinetic barrier to this reaction via eq 12 (Scheme 3) and subsequent $RE_{homo}$ (**TS7-11**) is 58.2 kJ mol$^{-1}$. Indeed, this barrier height is substantially above the energy of separated reactants for all computational methods used (see the Supporting Information, Table S1) and thus it would not be expected to occur in competition with the cross-coupling reaction (**TS8-9**, 26.0 kJ mol$^{-1}$). Thus, the origin of the cross-coupling selectivity is a noncompetitive barrier height (**TS7-11**, $RE_{homo}$) preventing reductive elimination to give the homocoupling product.

*Re-Formation of the Organocuprate via Decarboxylation and Mechanistic Summary.* As the kinetic barrier of decarboxylation is beneath the energy of the separated reactants (Figure 8), it is predicted that enough energy will be available in the system for a decarboxylation reaction to occur from the cross-coupling product ion (eq 7). As Figure 1b,c reveals, a small amount of decarboxylation occurs spontaneously, to form the active species dimethylcuprate at $m/z$ 93 and 96, respectively. However, the barrier to decarboxylation (145.2 kJ mol$^{-1}$ above the energy of the carboxylate[29]), together with collisional cooling of $[CH_3CuO_2CCH_3]^-$ by the helium bath gas, will limit the extent of this reaction under the reaction conditions used.

In summary, in the case of the allylic substrate allyl acetate, it was found experimentally that changing the LG from iodide to acetate the selectivity for cross-coupling is improved at the cost of slowing the reaction. These results are rationalized by DFT predictions, which show the reaction barriers to cross-coupling are increased in all cases in comparison with allyl iodide. These higher barriers would slow the reaction. The origin of selectivity was also found to be due to the raising of the kinetic barriers,


dx.doi.org/10.1021/om300717g | *Organometallics* XXXX, XXX, XXX−XXX

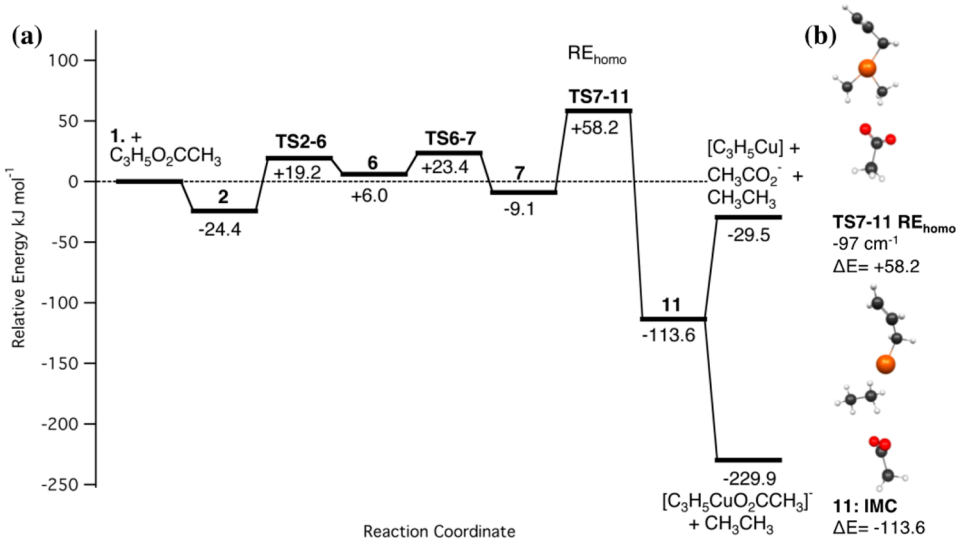


**Figure 7.** Calculated B3LYP/Def2-QZVP//B3LYP/SDD6-31+G(d): (a) relative energies (kJ mol$^{-1}$) for minima and transition states, relevant to bimolecular reactions of $[CH_3CuCH_3]^-$ + $C_3H_5O_2CCH_3$ via path D ($\pi$-addition) and homocoupling; (b) structures of minima and transition states relevant to bimolecular reactions of $[CH_3CuCH_3]^-$ + $C_3H_5O_2CCH_3$ via path D ($\pi$-addition) and homocoupling.

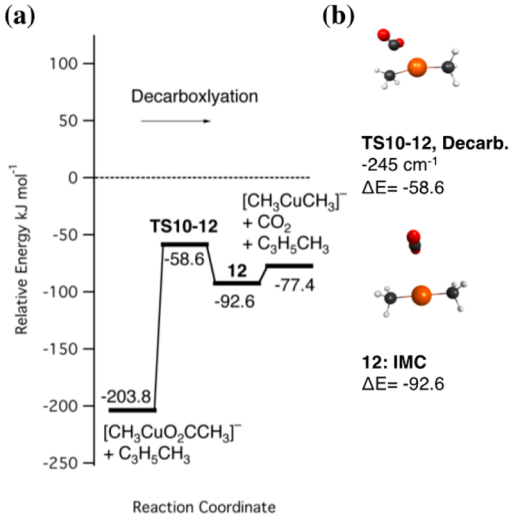


**Figure 8.** Calculated B3LYP/Def2-QZVP//B3LYP/SDD6-31+G(d) decarboxylation energies relative to the energies of the products formed from allylic alkylation.

with the homocoupling kinetic barrier being too high to be competitive with cross-coupling. The most viable pathway for the formation of a cross-coupled product was found to be path D, where the LG interacts with the metal center, thereby stabilizing the RE TS. The lack of LG loss in the IMR mass spectrum was also rationalized, as it becomes complexed to the metal center via path D. Thus, no free $CH_3CO_2^-$ is generated. This is an important step for a catalytic decarboxylative allylic alkylation. Given the observed consequences of leaving group on mechanism (for e.g. the change in $OA_\pi$), the next section focuses in more detail on the effects of changing the LG.

*Comparison of Leaving Group Effects.* The work so far has shown that switching the leaving group on the allylic substrate results in changes to both reactivity and selectivity (when LG = $I^-$, $CH_3CO_2^-$) for the allylic alkylation reaction with dimethylcuprate. A better understanding of the leaving group effects on this reaction may be gained from a systematic comparison of $C_3H_5LG$ (LG = $Cl^-$, $Br^-$, $I^-$, $CH_3CO_2^-$). The ability of an ion to act as a leaving group can be assessed via the gas-phase anion proton affinity (APA, eq 13), which is a measure of the intrinsic gas-phase basicity of the anion. The experimental values for APA for this series of leaving groups are given in Table 2 and highlight that the LG ability follows the order $CH_3CO_2^-$ < $Cl^-$ < $Br^-$ < $I^-$ (preferred).[27] It was of interest to determine whether the reactivity is a direct consequence of this ordering or if other factors (e.g., anion size, softness) were involved. Thus, key TS barriers to allylic alkylation for LG = $Cl^-$, $Br^-$, along with LG = $CH_3CO_2^-$, $I^-$ (Scheme 3), were calculated to assess if the predicted trend matched that of the LG APAs, and the data are also given in Table 2).

The calculated TS values show that kinetic barriers of $S_N2$ and $S_N2'$ type reactions increase with the APA of the leaving group in the order $CH_3CO_2^-$ > $Cl^-$ > $Br^-$ > $I^-$ (lowest kinetic barrier). This seems reasonable, given that the process of breaking the C−LG bond is concurrent with C−C bond formation. This trend has been noted previously for the reaction of a range of electrophiles in $S_N2$ reactions: for example, alkyl substrates with both halide and trifluoroacetate (TFA) leaving groups.[30] However, paths A and B are not the preferred mechanisms of reaction for cross-coupling for any of the electrophiles analyzed here.

The energetic trend for $OA_\sigma$ is qualitatively similar to the APA order. Indeed, the trend in charge distribution (Table 3) is consistent with the APA trend and accounts for the decrease in OA. On the basis of calculated values, the ordering of dipole moment magnitude is LG = $CH_3CO_2^-$ < $I^-$ < $Cl^-$ ≤ $Br^-$ (Table 3). In addition, while the molecular dipole moment for the halogenated molecules is oriented along the C−LG bond, the allyl acetate dipole is oriented perpendicular to the C−LG bond axis, due to the orientation of the oxygen atoms of the acetate group. Therefore, the halogenated molecules will favorably react due to both a larger dipole moment and direction of the dipole vector. Allyl iodide is the most reactive of these substrates, which falls outside the trend in dipole moments. It is more reactive than the other halides due to both its higher polarizabilty (Table 3) and its being a more effective leaving group (Table 2). Steric crowding by the LG may also hinder the TS $OA_\sigma$ for acetate more than for the halides.


dx.doi.org/10.1021/om300717g | *Organometallics* XXXX, XXX, XXX−XXX

**Table 2. Gas-Phase Experimental Anion Proton Affinities (APAs, eq 13, in kJ mol$^{-1}$) of Different LGs and Key TS Barriers (Scheme 3) for Cross-Coupling Calculated with B3LYP/SDDDef2-QZVP//B3LYP/SDD6-31+G(d)[a]**

| | | rel energy (kJ mol$^{-1}$) of TS barriers for allylic alkylation | | | | | | |
|---|---|---|---|---|---|---|---|---|
| | | | | path C | | path D (D′) | | |
| LG | APA (eq 13) (kJ mol$^{-1}$) | path A $S_N2$ | path B $S_N2'$ | $OA_\sigma$ | $RE_\sigma$ | $OA_\pi$ | $LG_{elim}$ | $RE_\pi$ |
| $CH_3CO_2^-$ | 1456 | 85.2 | 93.4 | 72.5 | 28.7 | 19.2 | 23.4 | 26.0 |
| $Cl^-$ | 1394.9 | 36.5 | 46.4 | 7.2 | −12.5 | 7.3 | −32.3 | −16.2 |
| $Br^-$ | 1353.9 | 17.4 | 27.2 | −13.5 | −27.0 | −6.6 | n/a | −29.9 |
| $I^-$ | 1315.24 | 2.2 | 11.4 | −27.3 | −37.5 | −26.0 | n/a | −45.4 |

[a]Energies are relative to separated reactants $[CH_3CuCH_3]^-$ and $C_3H_5LG$ (kJ mol$^{-1}$). APA values are from ref 27. n/a = not applicable.

**Table 3. B3LYP Calculated Properties Molecular Dipole Moment, Average Polarizability, and Charge Distribution for $C_3H_5LG$ (LG = $CH_3CO_2^-$, $Cl^-$, $Br^-$, $I^-$)**

| | | | calcd charge distribution (APT, H summed into heavy atoms) | | | |
|---|---|---|---|---|---|---|
| LG | dipole moment, $\mu$ (D) | av polarizability,[a] $\alpha_{av}$ (au) | $\alpha$-carbon | $\beta$-carbon | $\gamma$-carbon | LG |
| $CH_3CO_2^-$ | 2.04 | 67.8 | 0.49 | 0.02 | −0.02 | −0.49 |
| $Cl^-$ | 2.49 | 47.0 | 0.44 | −0.04 | 0.00 | −0.40 |
| $Br^-$ | 2.51 | 57.8 | 0.42 | −0.06 | 0.01 | −0.37 |
| $I^-$ | 2.24 | 66.1 | 0.36 | −0.06 | −0.00 | −0.31 |

[a]Average polarizabilty $\alpha_{av} = {}^1/_3(\alpha_{xx} + \alpha_{yy} + \alpha_{zz})$.[31]

The trend in $RE_\sigma$ is less affected by the LG anion. The anions are likely to alter the orbital symmetry and energies of the copper(III) TS complex via the vacant coordination site. The Lewis basicity, polarizability, and size of the LG anion are likely to be taking part in this process; however, the extent of involvement of each is not clear from the predictions here alone. Pathway C is a competitive reaction mechanism for LG = $Cl^-$, $Br^-$, $I^-$ but not for LG = $CH_3CO_2^-$, which is a consequence of a combination of LG attributes.

For $OA_\pi$, the effect of the leaving group is quite apparent by the change in mechanism upon moving down $Cl^-$ to $Br^-$ (Table 3). The two better LGs ($Br^-$ and $I^-$) dissociate directly in a concerted TS when forming the copper(III) intermediate. The two poorer LGs ($CH_3CO_2^-$ and $Cl^-$) react via a mechanism where intermediates are formed, which may subsequently dissociate via another TS. For LG = $Cl^-$, this is the rate-limiting step, and the loss of LG is facile. However, this is not the case for LG = acetate. This indicates $Cl^-$ is an intermediate LG. The change in mechanism is also apparent in the TS $OA_\pi$ geometries (Figure 9). While LG = $Br^-$, $I^-$ (Figure 9c,d) have similar TS geometries and imaginary vibrations, LG = $CH_3CO_2^-$ is considerably different, where the addition is more symmetrical and akin to olefin addition, without concurrent loss of the LG. LG = $Cl^-$ shares characteristics of both TS types mentioned above, being most like the TS for LG = $CH_3CO_2^-$, forming an intermediate where the LG has not dissociated. In solution-phase NMR experiments, differences in reactivity between allyl chloride and allyl acetate with dimethylcuprate that were ascribed to the reaction mechanism have also been observed.[32]

The TS $RE_\pi$ species for all four LGs are similar in energy to those of the TS $RE_\sigma$. It also unclear here what role the LG anion plays on lowering the TS $RE_\pi$. It is again likely that anion size and polarizabilty contribute to the metal orbital symmetry and energies in the TS, although to what extent is not yet clear. The reaction via path D is thus dependent on leaving group ability and, to a lesser extent, the ability to assist in RE. The nature of this TS will also determine whether the LG is transferred to the metal center.

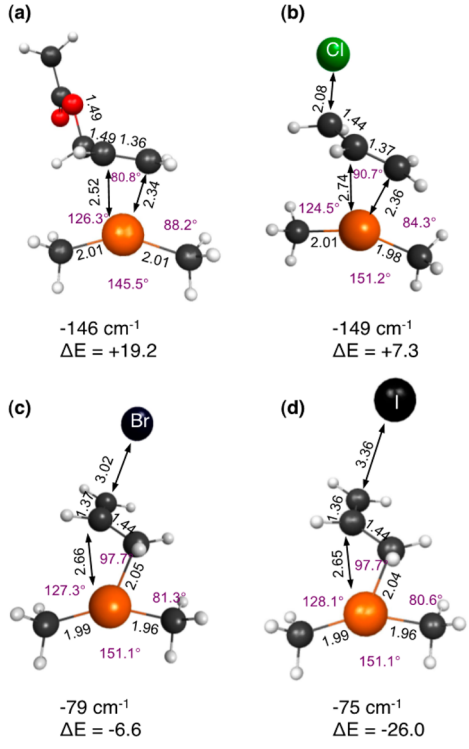


**Figure 9.** Comparison of TS $OA_\pi$ for $[CH_3CuCH_3]^-$ + $C_3H_5LG$, with LG = (a) $CH_3CO_2$, (b) Cl, (c) Br, and (d) I. The energy ($\Delta E$) is in kJ mol$^{-1}$.

To assess how the selectivity changes with LG, the TS for $RE_{homo}$ was also calculated (Table 4). These results show that selectivity is indeed improved at the cost of reactivity, LG = $Cl^-$, $CH_3CO_2^-$ are less reactive, and $RE_{homo}$ is not competitive with cross-coupling, while the more reactive LG = $I^-$, $Br^-$ are predicted to yield some homocoupling side product.


dx.doi.org/10.1021/om300717g | Organometallics XXXX, XXX, XXX−XXX

**Table 4. Predicted Homocoupling Kinetic Barriers with LG = $CH_3CO_2^-$, $Cl^-$, $Br^-$, $I^-$ Calculated with B3LYP/SDDDef2-QZVP//B3LYP/SDD6-31+G(d)[a]**

| LG | TS to homocoupling rel energy (kJ $mol^{-1}$) $RE_{homo}$ |
|---|---|
| $CH_3CO_2^-$ | 58.2 |
| $Cl^-$ | *b* |
| $Br^-$ | −10.0 |
| $I^-$ | −30.0 |

[a]Energies are relative to separated reactants $[CH_3CuCH_3]^-$ and $C_3H_5LG$ (kJ $mol^{-1}$). [b]No TS to $RE_{homo}$ located.

In summary, iodide is more reactive as a leaving group, while $CH_3CO_2^-$ is more selective but less reactive. A previous mechanistic study has compared the reactivity of cuprates with the alkyl halide electrophiles $CH_3I$ and $CH_3Br$ and found an analogous trend.[33] However, the allylic alkylation reaction is not as simple as this example, with the net effect on the Cu(III) intermediate likely to be important where this is the rate-limiting step, rather than the LG ability on the OA step alone. This is highlighted by the change in the $OA_\pi$ TS (Figure 9), where clear differences in mechanism due to the LG substituent are observed.

## CONCLUSIONS

The first gas-phase catalytic cycle for decarboxylative allylic alkylation has been demonstrated using a combination of mass spectrometry experiments and DFT calculations. Dimethylcuprate, $[CH_3CuCH_3]^-$, was shown to undergo a cross-coupling reaction with allyl acetate and LG ($CH_3CO_2^-$) was selectively transferred to the metal center to generate $[CH_3CuO_2CCH_3]^-$ (step 1 of Scheme 1). This step is directly related to allylic alkylation reactions previously observed between allylic esters and cuprates in the condensed phase.[9−11] Decarboxylation of $[CH_3CuO_2CCH_3]^-$ regenerates the dimethylcuprate catalyst, $[CH_3CuCH_3]^-$ (step 2 of Scheme 1), thereby closing a simple two-step catalytic cycle. While it is interesting to note that copper-catalyzed decarboxylation reactions are well-known (cf. step 2 of Scheme 1),[3] it appears that the combination of copper-mediated allylic alkylation reactions and copper-catalyzed decarboxylation has not been previously examined. Our results suggest it would be fruitful to examine condensed-phase copper-catalyzed decarboxylative allylic alkylation reactions.

Finally, we have used DFT calculations to examine the role of the LG in cross-coupling reactions between dimethylcuprate and allylic substrates (where LG = $CH_3CO_2^-$, $Cl^-$, $Br^-$, $I^-$). It was found that gas-phase anion proton affinities account for some of the reactivity trends, particularly when the reaction was concerted. However, the lowest energy cross-coupling reaction mechanisms are predicted to be multistep, involving copper(III) intermediates. The effect of the LG on reductive elimination from these intermediates is complex and cannot be accounted for by a simplistic APA-based reactivity model, unlike the case for previous gas-phase examples involving primary alkyl halides, where the C−LG bond breaking was part of the rate-limiting step. A combination of LG attributes is likely to play a role in the reaction outcomes of allylic alkylation reactions with organocuprates. Overall, changing the LG in order to improve selectivity comes at the cost of reactivity.

## ASSOCIATED CONTENT

### Supporting Information

Text, figures, and tables giving IMR mass spectra with copper isotope $^{65}Cu$, Cartesian coordinates, energies, and vibrational frequencies for reactants, intermediates, products, and transition states, an M06 and B2PLYPD energy comparison, high-resolution MS data, and the full citation for ref 18. This material is available free of charge via the Internet at http://pubs.acs.org.

## AUTHOR INFORMATION

### Corresponding Author

*Tel: +61 3 8344-2452. Fax: +61 3 9347-5180. E-mail: rohair@unimelb.edu.au.

### Notes

The authors declare no competing financial interest.

## ACKNOWLEDGMENTS

We thank the ARC for financial support via grant DP110103844 (to R.A.J.O.). N.J.R. thanks the Faculty of Science for both (1) a Science Faculty Scholarship and (2) an Albert Shimmins Postgraduate Writing-Up Award. The VICS is acknowledged for the Chemical Sciences High Performance Computing Facility (Gomberg).

## REFERENCES

(1) For example, decarboxylative coupling can yield stilbenes: Chamchaang, W.; Chantarasiri, N.; Chaona, S.; Thebtaranonth, C.; Thebtaranonth, Y. *Tetrahedron* **1984**, *40*, 1727−1730.

(2) (a) Hurd, C. D.; Blunck, F. H. *J. Am. Chem. Soc.* **1938**, *60*, 2419−2425. (b) Mackinnon, H. M.; Ritchie, P. D. *J. Chem. Soc.* **1957**, 2564−2569. (c) Taylor, R. In *Acid Derivatives*; Patai, S., Ed.; Wiley: Chichester, U.K., 1979; pp 859−914.

(3) (a) Goossen, L. J.; Collet, F.; Goossen, K. *Isr. J. Chem.* **2010**, *50*, 617−629. (b) Rodriguez, N.; Goossen, L. *J. Chem. Soc. Rev.* **2011**, *40*, 5030−5048. (c) Shang, R.; Liu, L. *Sci. China: Chem.* **2011**, *54*, 1670−1687. (d) Cornella, J.; Larrosa, I. *Synthesis* **2012**, 653−676. (e) Dzik, W. I.; Lange, P. P.; Goossen, L. J. *Chem. Sci.* **2012**, *3*, 2671−2678.

(4) Weaver, J. D.; Recio, A.; Grenning, A. J.; Tunge, J. A. *Chem. Rev.* **2011**, *111*, 1846−1913.

(5) (a) Heim, A.; Terpin, A.; Steglich, W. *Angew. Chem., Int. Ed.* **1997**, *36*, 155−156. (b) Goosen, L. J.; Deng, G.; Levy, L. M. *Science* **2006**, *313*, 662−664. (c) Shepard, A. F.; Winslow, N. R.; Johnson, J. R. *J. Am. Chem. Soc.* **1930**, *52*, 2083−2090.

(6) Rijs, N. J.; Yoshikai, N.; Nakamura, E.; O'Hair, R. A. J. *J. Am. Chem. Soc.* **2012**, *134*, 2569−2580.

(7) (a) Alexakis, A.; Backvall, J. E.; Krause, N.; Pamies, O.; Dieguez, M. *Chem. Rev.* **2008**, *108*, 2796−2823. (b) Harutyunyan, S. R.; den Hartog, T.; Geurts, K.; Minnaard, A. J.; Feringa, B. L. *Chem. Rev.* **2008**, *108*, 2824−2852. (c) Falciola, C. A.; Alexakis, A. *Eur. J. Org. Chem.* **2008**, *2008*, 3765−3780.

(8) (a) James, P. F.; O'Hair, R. A. J. *Org. Lett.* **2004**, *6*, 2761−2764. (b) Rijs, N.; Khairallah, G. N.; Waters, T.; O'Hair, R. A. J. *J. Am. Chem. Soc.* **2008**, *130*, 1069−1079.

(9) Rona, P.; Tokes, L.; Tremble, J.; Crabbe, P. J. *J. Chem. Soc., Chem. Commun.* **1969**, 43−44.

(10) (a) Anderson, R. J.; Henrick, C. A.; Siddall, J. B. *J. Am. Chem. Soc.* **1970**, *92*, 735−737. (b) Goering, H. L.; Singleton, V. D. *J. Am. Chem. Soc.* **1976**, *98*, 7854−7855.

(11) Levisalles, J.; Rudler-Chauvin, M.; Rudler, H. *J. Organomet. Chem.* **1977**, *136*, 103−110.

(12) Yoshikai, N.; Zhang, S. L.; Nakamura, B. *J. Am. Chem. Soc.* **2008**, *130*, 12862−12863.

(13) For the first report of a transition-metal-catalyzed reaction in the gas phase see: (a) Kappes, M. M.; Staley, R. H. *J. Am. Chem. Soc.* **1981**, *103*, 1286−1287. For selected examples of gas-phase catalytic cycles see: (b) Waters, T.; Khairallah, G. N.; Wimala, S. A. S. Y.; Ang, Y. C.; O'Hair, R. A. J.; Wedd, A. G. *Chem. Commun.* **2006**, 4503−4505. (c) Waters, T.; Wedd, A. G.; O'Hair, R. A. J. *Chem. Eur. J.* **2007**, *13*, 8818−8829. (d) Harris, B. L.; Waters, T.; Khairallah, G. N.; O'Hair, R. A. J. *J. Phys. Chem. A*, in press (dx.doi.org/10.1021/jp3046142).

(e) Lang, S. M.; Bernhardt, T. M.; Barnett, R. N.; Landman, U. *Angew. Chem., Int. Ed.* **2010**, *49*, 980−983. (f) Lang, S. M.; Bernhardt, T. M.; Barnett, R. N.; Landman, U. *J. Phys. Chem. C* **2011**, *115*, 6788−6795. For reviews of catalytic cycles studied in the gas phase see: (g) Waters, T.; O'Hair, R. A. J. In *The Encyclopedia of Mass Spectrometry*; Nibbering, N. M. M., Ed.; Elsevier: Oxford, U.K., 2005; Vol. 4 (Fundamentals of and Applications to Organic (and Organometallic) Compounds), pp 604−612. (h) Bohme, D. K.; Schwarz, H. *Angew. Chem., Int. Ed.* **2005**, *44*, 2336−2354. (i) Schwarz, H. *Angew. Chem., Int. Ed.* **2011**, *50*, 10096−10115. (j) Castleman, A. W., Jr. *Catal. Lett.* **2011**, *141*, 1243−1253. (k) Lang, S. M.; Bernhardt, T. M. *Phys. Chem. Chem. Phys.* **2012**, *14*, 9255−9269. (l) Schlangen, M.; Schwarz, H. *Catal. Lett.*, in press (DOI 10.1007/s10562-012-0892-3).

(14) (a) Waters, T.; O'Hair, R. A. J.; Wedd, A. G. *J. Am. Chem. Soc.* **2003**, *125*, 3384−3396. (b) O'Hair, R. A. J. *Chem. Commun.* **2006**, 1469−1481. (c) Gronert, S. *J. Am. Soc. Mass Spectrom.* **1998**, *9*, 845−848.

(15) (a) Donald, W. A.; McKenzie, C. J.; O'Hair, R. A. J. *Angew. Chem., Int. Ed.* **2011**, *50*, 8379−8383. (b) Lam, A. K. Y.; Li, C.; Khairallah, G.; Kirk, B. B.; Blanksby, S. J.; Trevitt, A. J.; Wille, U.; O'Hair, R. A. J.; da Silva, G. *Phys. Chem. Chem. Phys.* **2012**, *14*, 2417−2426.

(16) The accuracy of these ion trap rate measurements was checked by measuring the known rate constant for the reaction $Br^- + CH_3I \rightarrow CH_3Br + I^-$, which has been determined at room temperature previously in a flowing afterglow apparatus: Gronert, S.; DePuy, C. H.; Bierbaum, V. M. *J. Am. Chem. Soc.* **1991**, *113*, 4009−4010.

(17) (a) Su, T.; Bowers, M. T. *Int. J. Mass Spectrom. Ion Phys.* **1973**, *12*, 347−356. (b) Lim, K. F. *Quantum Chem. Program Exch.* **1994**, *14*, 3.

(18) Frisch, M. J.; et al. *Gaussian 09, Revisions B.01, C.01*; Gaussian, Inc., Wallingford, CT, 2010.

(19) (a) Becke, A. D. *J. Chem. Phys.* **1993**, *98*, 5648−5652. (b) Lee, C.; Yang, W.; Parr, R. G. *Phys. Rev. B: Condens. Matter* **1988**, *37*, 785−789.

(20) (a) Dolg, M.; Wedig, U.; Stoll, H.; Preuss, H. *J. Chem. Phys.* **1987**, *86*, 866−872. (b) Hariharan, P. C.; Pople, J. A. *Theor. Chim. Acta* **1973**, *28*, 213−222. (c) Clark, T.; Chandrasekhar, J.; Schleyer, P. v. R. *J. Comput. Chem.* **1983**, *4*, 294−301. (d) Krishnan, R.; Binkley, J. S.; Seeger, R.; Pople, J. A. *J. Chem. Phys.* **1980**, *72*, 650−654. (e) Gill, P. M. W.; Johnson, B. G.; Pople, J. A.; Frisch, M. J. *Chem. Phys. Lett.* **1992**, *197*, 499−505.

(21) (a) Weigend, F.; Ahlrichs, R. *Phys. Chem. Chem. Phys.* **2005**, *7*, 3297−3305. (b) Weigend, F.; Furche, F.; Ahlrichs, R. *J. Chem. Phys.* **2003**, *119*, 12753−12762. Basis sets were obtained from the EMSL Basis Set Library via the Basis Set Exchange: (c) Schuchardt, K. L.; Didier, B. T.; Elsethagen, T.; Sun, L.; Gurumoorthi, V.; Chase, J.; Li, J.; Windus, T. L. *J. Chem. Inf. Model.* **2007**, *47*, 1045−1052.

(22) Zhao, Y.; Truhlar, D. G. *Theor. Chem. Acc.* **2008**, *120*, 215−241.

(23) (a) Grimme, S. *J. Chem. Phys.* **2006**, *124*, 034108. (b) Schwabe, T.; Grimme, S. *Phys. Chem. Chem. Phys.* **2007**, *9*, 3397−3406.

(24) Bode, B. M.; Gordon, M. S. *J. Mol. Graph. Model.* **1998**, *16*, 133−138.

(25) For discussions of isotope effects in mass spectrometry experiments see: (a) Derrick, P. J. *Mass Spectrom. Rev.* **1983**, *2*, 285−298. (b) Lehman, T. A. *Mass Spectrom. Rev.* **1995**, *14*, 353−382. For a recent review of isotope effects in organometallic chemistry see: (c) Gómez-Gallego, M.; Sierra, M. A. *Chem. Rev.* **2011**, *111*, 4857−4963.

(26) Rijs, N. J.; Sanvido, G. B.; Khairallah, G. N.; O'Hair, R. A. J. *Dalton Trans.* **2010**, *39*, 8655−8662.

(27) Gas-phase anion proton affinities (APAs) are from the NIST website (http://webbook.nist.gov, retrieved Sept 2012).

(28) Anslyn, E. V.; Dougherty, D. A. In *Modern Physical Organic Chemistry*; University Science Books: Sausalito, CA, 2006; pp 288−296.

(29) The barrier to decarboxylation (eq 7) previously reported in ref 8a has been recalculated at the B3LYP/Def2-QZVP//B3LYP/SDD6-31+G(d) level of theory. It is 145.2 kJ $mol^{-1}$, while the overall endothermicity for decarboxylation to form the separated products, $[CH_3CuCH_3]^- + CO_2$ (eq 7), is 126.4 kJ $mol^{-1}$.

(30) Gronert, S.; Fagin, A. E.; Okamoto, K.; Mogali, S.; Pratt, L. M. *J. Am. Chem. Soc.* **2004**, *126*, 12977−12983.

(31) Sim, F.; Salahub, D. R.; Chin, S. *Int. J. Quantum Chem.* **1992**, *43*, 463−479.

(32) Bartholomew, E. R.; Bertz, S. H.; Cope, S.; Murphy, M.; Ogle, C. A. *J. Am. Chem. Soc.* **2008**, *130*, 11244−11245.

(33) Mori, S.; Nakamura, E.; Morokuma, K. *J. Am. Chem. Soc.* **2000**, *122*, 7294−7307.